Available online at www.sciencedirect.com
SCIENCE DIRECT
Journal of Power Sources 150 (2005) 32–47
JOURNAL OF POWER SOURCES
www.elsevier.com/locate/jpowsour

Dynamic modeling of solid oxide fuel cell: The effect of diffusion and inherent impedance

Yutong Qi, Biao Huang*, Karl T. Chuang

Department of Chemical and Materials Engineering, University of Alberta, Edmonton, Alberta, Canada T6G 2G6

Received 21 January 2005; received in revised form 28 February 2005; accepted 28 February 2005
Available online 10 May 2005

Abstract

With the aim of dynamic simulation and control, a cell-level nonlinear state-space dynamic model of solid oxide fuel cell (SOFC) based on physical principles is built. It demonstrates that reactant diffusion processes from gas flow bulks to triple phase boundaries (tpb) play an important role in the dynamic behaviors of SOFC. The simulation shows that under certain condition, the effect of the double layer capacitance may be neglected. The phenomenon of slow rise of voltage in current interrupt experiment may be explained by the dynamic behaviors of partial pressures in the vicinity immediately above tpbs. A new equivalent circuit is proposed. The results are demonstrated through simulations.

Keywords: SOFC; Dynamic modeling; Simulation; Diffusion; Impedance

1. Introduction

Solid oxide fuel cell (SOFC) is a type of fuel cells identified as the likely fuel cell technologies that will capture the most significant market in the future. SOFC uses a special solid oxide cermet (mostly yttria-stabilized zirconia, YSZ) as the electrolyte and usually works at a high temperature, in the range of 800–1000 °C to reach the electrolytes ionic conductivity requirement. A large amount of literature has been published about SOFCs as well as other fuel cells. Most of the work has focused on investigating static electrochemical characteristics, such as reaction mechanisms, state-of-the-art cell components, new materials, etc. For the purpose of dynamic simulation and control, the dynamic characteristics of fuel cell must be understood. In this paper, a dynamic model of SOFC at cell-level is proposed to investigate the dynamic properties of fuel cells.

In order to investigate dynamic characteristics of SOFC, some dynamic modeling and simulations have been performed on molecular scale [1,2]. However, such micro-dynamic models are not suitable for macro-applications.

Early macro-dynamic modeling of SOFC was performed by Achenbach [3,4]. He examined the transient cell voltage performance of a cross-flow planar SOFC cell due to the temperature changes and the perturbations in current density.

The dynamic model given by Padullés et al. [5] included the species dynamics on stack-level the first time. Zhu and Tomsovic [6] adopted the model of Padullés et al. [5] for analyzing the load-following performance of microturbines and fuel cells. Sedghisigarchi and Feliachi [7] combined Achenbachs heat transfer dynamics and Padullés' species dynamics, and performed dynamic simulations. However, in these models, only lumped dynamic behavior of species along the fuel/air channel is considered. The processes of species transport from flow bulk to triple phase boundary (tpb) have not been considered.

The model proposed in this paper is a cell-level species dynamic model. It lies between micro- and macro-scale. Because behavior of stack is determined by that of cells, the cell-level model is a building block for a stack-level model. Dynamic behaviors of voltage, current, gas consumption rates controlled by different load and partial pressures are demonstrated through simulations.

* Corresponding author. Tel.: +1 780 492 9016; fax: +1 780 492 2881.
E-mail address: biao.huang@ualberta.ca (B. Huang).

0378-7753/$ – see front matter © 2005 Elsevier B.V. All rights reserved.
doi:10.1016/j.jpowsour.2005.02.080

Nomenclature

a_{H_2}	activity of hydrogen
a_{H_2O}	activity of water vapor
a_{O_2}	activity of oxygen
A	area (m^2)
C	concentration ($mol\,m^{-3}$)
C_{ct}	charge transfer capacity (F)
D	diffusion coefficient ($m^2\,s^{-1}$)
E	voltage (V)
$E_{act,a}$	anode reaction activation energy ($J\,mol^{-1}$)
$E_{act,c}$	cathode reaction activation energy ($J\,mol^{-1}$)
F	Faradays constant (=96487 $C\,mol^{-1}$)
$\Delta\bar{g}_f$	Gibbs free energy released ($J\,mol^{-1}$)
i	cell current (A)
i_l	current limit (A)
i_0	exchange current (A)
J^s	consumption rate flowing into the outer surface of diffusion layer ($\mu mol\,s^{-1}$)
J^r	reaction rate at reaction sites ($\mu mol\,s^{-1}$)
j	diffusion flux ($\mu mol\,s^{-1}\,m^{-2}$)
L_a	thickness of anode diffusion layer (m)
L_c	thickness of cathode diffusion layer (m)
M	mole mass ($g\,mol^{-1}$)
p^b	partial pressure in gas bulk (atm)
p^{tpb}	partial pressure in the immediate vicinity of tpbs (atm)
P	pressure (atm)
P^0	standard pressure (atm)
$P^0_{H_2O}$	vapor pressure of the steam at the temperature considered (atm)
R	gas constant ($= 82.05 \times 10^{-5}\,J\,mol^{-1}\,K^{-1}$)
R_{ct}	charge transfer resistance (Ω)
R_{load}	load resistance (Ω)
R_o	ohmic resistance (Ω)
s	Laplace operator
T	temperature (K)
V	voltage (V)
V_{out}	fuel cell voltage out (V)

Greek letters

ε	porosity
η_{act}	activation loss (V)
τ	tortuosity
$(\sum \nu_i)$	diffusional volumes

Superscripts

0	at standard pressure
b	gas flow bulk
r	flow at the reaction site
s	flow at the upper surface of diffusion layer
tpb	triple phase boundary

Subscripts

12	binary diffusion
a	anode
act	activation
c	cathode
ct	charge transfer
eff	effective
H_2	hydrogen
H_2O	water vapor
k	Knudsen
load	load
N_2	nitrogen
o	ohmic
out	output
O_2	oxygen

The remainder of this paper is organized as follows: the principle of SOFC is discussed in Section 2. The dynamic modeling is discussed in Section 3. Relational parameters are shown in Section 4. Simulation results and analysis are given in Section 5, followed by conclusions in Section 6.

2. Fuel cell principles

A typical H_2–H_2O,Ni|YSZ|Pt,O_2 fuel cell is shown in Fig. 1. The chemical reactions inside the cell that are directly involved in the production of electricity are

$$\begin{aligned} &\text{at anode tpb:} \quad H_2 + O^{2-} \rightarrow H_2O + 2e^-, \\ &\text{at cathode tpb:} \quad \tfrac{1}{2}O_2 + 2e^- \rightarrow O^{2-} \end{aligned} \tag{1}$$

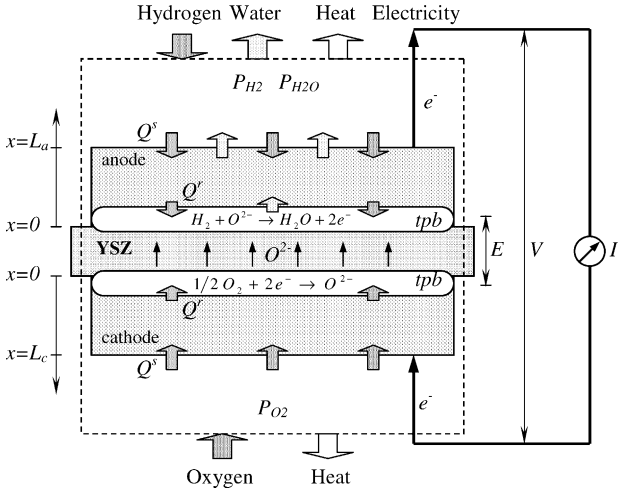

Fig. 1. Principle of solid oxide fuel cell.

2.1. Voltage output

In the ideal situation (reversible), electrical work is equal to the Gibbs free energy released $\Delta\bar{g}_f$, i.e.

$$\Delta\bar{g}_f = -2FE \tag{2}$$

The electromotive force (EMF) or reversible open circuit voltage E of the hydrogen fuel cell is given as

$$E = -\frac{\Delta\bar{g}_f}{2F} \tag{3}$$

where F is Faraday constant.

Partial pressures or gas concentrations affect EMF through the Nernst equation [8]:

$$E = E^0 + \frac{RT}{2F}\ln\left(\frac{a_{H_2}a_{O_2}^{0.5}}{a_{H_2O}}\right) \tag{4}$$

where a_{H_2}, a_{O_2} and a_{H_2O} are activities. If gases behave as ideal gases, the activities are

$$a_{H_2} = \frac{p_{H_2}}{P^0}, \qquad a_{O_2} = \frac{p_{O_2}}{P^0}, \qquad a_{H_2O} = \frac{p_{H_2O}}{P^0_{H_2O}}$$

where p_{H_2}, p_{O_2}, and p_{H_2O} are reactant partial pressures, P^0 is the standard pressure, $P^0_{H_2O}$ is the vapour pressure of the steam at the temperature concerned. E is also called Nernst voltage. If $P^0 = P^0_{H_2O} = 1$, the equation can be simplified to

$$E = E^0 + \frac{RT}{2F}\ln\left(\frac{p_{H_2}p_{O_2}^{1/2}}{p_{H_2O}}\right) \tag{5}$$

Irreversibilities reduce the cells voltage. They are mainly activation loss, ohmic loss and concentration loss. The voltage is usually modeled in the steady state form [8]:

$$V = E - iR_{in} - A\ln\left(\frac{i}{i_0}\right) - B\ln\left(1 - \frac{i}{i_l}\right) \tag{6}$$

where i is the current produced by the cell. R_{in} is the inherent resistance of the fuel cell. i_0 is the exchange current, an important parameter of weighting the activity of catalyst reaction. i_l is the limiting current, at which the fuel is used up at a rate equal to its maximum supply rate. A and B are coefficients. The second term in the equation represents the ohmic loss; the third term is activation loss and the fourth term represents the concentration loss.

2.2. Current output

Neglecting the transit dynamics of the reactions, the relation between current and reactions can be expressed as [8]:

$$i = 2FJ^r_{H_2} = 2FJ^r_{H_2O} = 4FJ^r_{O_2} \tag{7}$$

where superscript r represents the fuel consumption or water vapor production rate at tpbs.

The maximum current that a cell can output is limited by several factors.

The first one is reactant supply rates. In cell-level, they are controlled by concentration gradients between tpbs and gas flow bulks. When the current output increases, the hydrogen and oxygen concentrations at tpbs decrease to create larger concentration gradients. Once one of them decreases to zero, the supply rate reaches its maximum. Current can not be increased anymore, and it is the maximum current fuel cell can provide. Under this condition, the voltage drops to zero as described by Nernst equation.

Second, current output is also limited by reaction rates and the area where reactions take place. In most cases, reactions are fast in anode. However, because cathode reaction is slow [9], current output is also limited by the maximum ion production rate.

Third, current output is controlled by voltage and load impedance.

Fourth, maximum current is limited by ionic conductivity of electrolyte. It follows Ohm's law. The limitation resistance usually merged into the inherent impedance. In normal operating ranges, the reactions usually do not reach the limits mentioned before. Thus, the current is determined mainly by Ohm's law.

2.3. Dynamic process of fuel cell

When fuel gases are fed to cell, they must flow through the gas boundary layers, porous support layers and porous electrodes to tpbs, where reactions take place. Neglecting the reaction dynamics, these mass transport processes are the main dynamic sources of the fuel cells operated under the uniform temperature condition. The dynamics of fuel cell including rate determination steps etc. may be expressed by transfer function block diagram, shown in Fig. 2.

Another important source that affects fuel cell's dynamic behavior is its inherent impedance. Fuel cell including SOFCs inherent impedance is well studied via electrochemical impedance spectroscopy (EIS) method [10–16]. They can be simplified as equivalent RC circuits. So the effect of inherent impedance to voltage and current dynamic behavior is similar to a RC filter.

3. Modeling approach

3.1. Assumptions

In this paper, we focus on dynamic behavior of SOFC due to the diffusion and impedance. We consider two scenarios: (1) an elemental volume of the cell, and (2) a cell with uniform temperature. The results derived from this paper are valid for both scenarios. This serves for two purposes: (1) when consider an elemental volume of SOFC, the assumption of uniform temperature condition is valid and dynamic behavior of an elemental SOFC can be used as a building block for

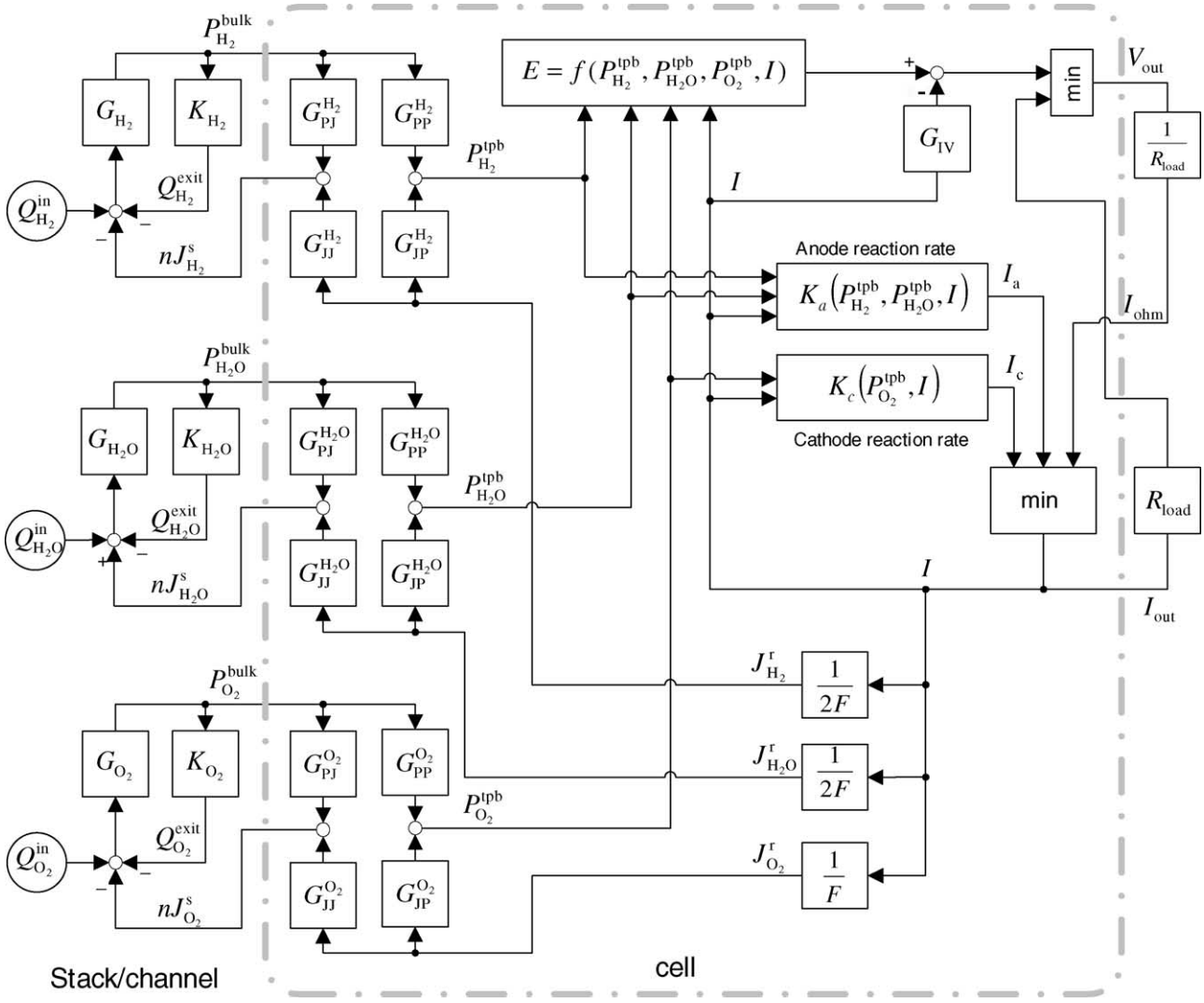

Fig. 2. Schematic block diagram of fuel cell.

a complete cell dynamic model when the temperature varies along the cell; (2) if consider a whole cell operating under uniform temperature instead, we actually isolate and investigate SOFC cell dynamics due to diffusion and impedance alone. The dynamic responses are due to the effect of diffusion and impedance only and should not be interpreted as the complete dynamic responses of the cell.

The following are the assumptions if we consider an elemental volume of the cell:

(1) An elemental volume of H_2–H_2O,Ni|YSZ|LSM, air cell [12]. The definition of the elemental volume in different SOFC cells is shown in Fig. 3.
(2) Cell's external load is a pure resistance.
(3) Temperature is uniform throughout the elemental volume.
(4) Gas partial pressures in flow bulks surrounding the elemental volume are uniform.

3.2. I/O variables

The aim of the model to be developed is to describe the external characteristics. So input variables are related to inputs of SOFC. Output variables are cell's power outputs, such as voltage, current, etc.

The input–output variables are shown in Table 1. The first input variable is the external load. Under the normal operating conditions, it is external load that determines the current output *i* and so affects the reaction. Different load impedance affects the output properties in different way. In order to investigate the basic dynamic behavior of the current output, load impedance is assumed to be a pure resistance R_{load} in the model.

Other input variables are partial pressures of reactants in gas bulks. They affect the reactant supplies and reaction rates directly. For a single cell under normal operating condition, reactant concentrations or partial pressures affect

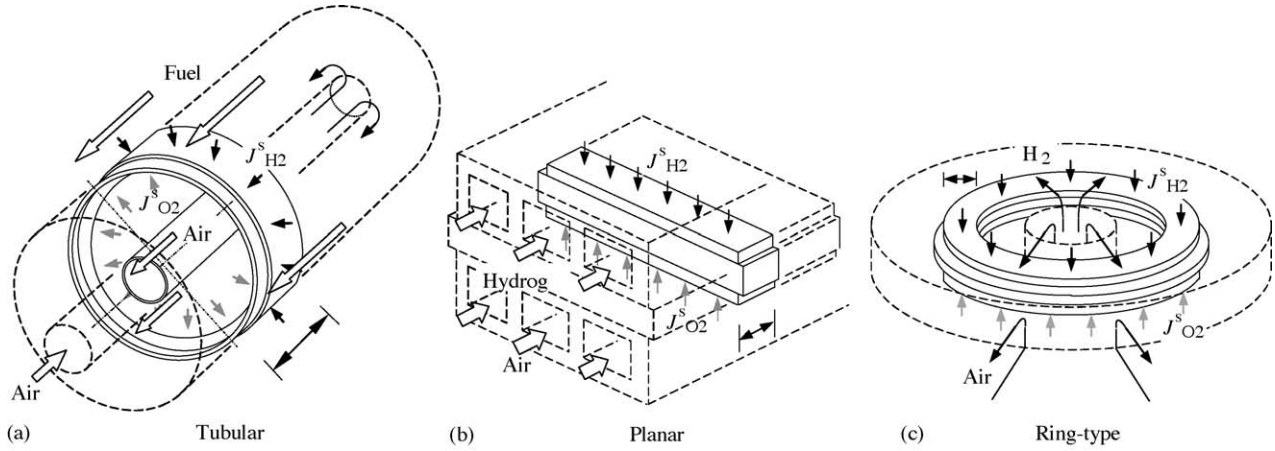

Fig. 3. Definition of finite volume in different SOFC cells.

the diffusion processes and the Gibbs free energy, and thus the voltage. Therefore, other input variables are $p^{b}_{H_2}$, $p^{b}_{H_2O}$, and $p^{b}_{O_2}$.

Output variables of the model include potential difference exerted on the load resistance, V_{out}, current flow through the load resistance, i, H_2 and O_2 consumption rates, $J^{s}_{H_2}$, $J^{s}_{O_2}$, and water production rate $J^{s}_{H_2O}$.

3.3. Diffusion

The path of mass transport from the flow bulk to the reaction site involves two stages. First, from the flow bulk to the cell surface layer. Second, through the porous electrode to reaction sites [17]. In the first stage, mass flux diffuses through the boundary layer to the cell surface. In the second stage, mass flux diffuses inside the porous electrode. In all these two stages, diffusion is the main means of mass transport.

One of the most widely used diffusion models is Fick's law:

$$j = -D\frac{\mathrm{d}C}{\mathrm{d}x} \tag{8}$$

Table 1
Input and output variables

Inputs	
R_{load}	Load resistance
$p^{b}_{H_2}$	Partial pressure of hydrogen in anode gas bulk
$p^{b}_{O_2}$	Partial pressure of oxygen in cathode gas bulk
$p^{b}_{H_2O}$	Partial pressure of water vapor in anode gas bulk
Outputs	
V_{out}	Voltage output of SOFC cell
i	Current output of SOFC cell
$J^{s}_{H_2}$	Hydrogen consumption rate of SOFC cell
$J^{s}_{O_2}$	Oxygen consumption rate of SOFC cell
$J^{s}_{H_2O}$	Hydrogen consumption rate of SOFC cell

The mass transport equation can be written as

$$\frac{\partial C}{\partial t} = D\frac{\partial^2 C}{\partial x^2} \tag{9}$$

where C is the mass concentration, D the diffusion coefficient, A the diffusion cross-sectional area, and x is the diffusion depth as defined in Fig. 1.

Fick's law shows that concentration is dependent on diffusion thickness. In order to get the concentrations at tpbs, one usually applies the finite element method [18–22]. However, by means of Laplace transform, the analytical dynamic relations can be expressed in the form of transfer functions without involving spacial variables.

3.3.1. Developing mass transport transfer function

Perform Laplace's transform in Eq. (9) to convert the partial differential equation to the ordinary differential equation [23]:

$$\frac{\mathrm{d}^2 C(s)}{\mathrm{d}x^2} - \frac{s}{D}C(s) = 0 \tag{10}$$

Boundary conditions are

$$j^{r}(s) = -D\frac{\mathrm{d}C(s)}{\mathrm{d}x}|_{x=0}, \qquad C^{b}(s) = C(s)|_{x=L} \tag{11}$$

Solving Eq. (10) yields:

$$C(s)(x) = \frac{C^{b}(s) + \frac{j^{r}(s)}{\sqrt{Ds}}\exp\left(-\sqrt{\frac{s}{D}}L\right)}{\exp\left(\sqrt{\frac{s}{D}}L\right) + \exp\left(-\sqrt{\frac{s}{D}}L\right)}\exp\left(\sqrt{\frac{s}{D}}x\right) + \frac{C^{b}(s) - \frac{j^{r}(s)}{\sqrt{Ds}}\exp\left(\sqrt{\frac{s}{D}}L\right)}{\exp\left(\sqrt{\frac{s}{D}}L\right) + \exp\left(-\sqrt{\frac{s}{D}}L\right)}\exp\left(-\sqrt{\frac{s}{D}}x\right) \tag{12}$$

Assume that the gases are ideal gases and the flow area is A. At tpbs where $x = 0$, the partial pressure in the vicinity of

tpb is

$$p^{\mathrm{tpb}}(s) = -\frac{\exp\left(\sqrt{\frac{s}{D}}L\right) - \exp\left(-\sqrt{\frac{s}{D}}L\right)}{\exp\left(\sqrt{\frac{s}{D}}L\right) + \exp\left(-\sqrt{\frac{s}{D}}L\right)} \frac{1}{\sqrt{Ds}} \frac{RT}{A} J^{\mathrm{r}}(s) + \frac{2}{\exp\left(\sqrt{\frac{s}{D}}L\right) + \exp\left(-\sqrt{\frac{s}{D}}L\right)} p^{\mathrm{b}}(s) \quad (13)$$

On the surface of the diffusion layer, mass flow rate is $J^{\mathrm{s}} = AD(\mathrm{d}C/\mathrm{d}x)|_{x=L}$. The dynamic relation is

$$J^{\mathrm{s}}(s) = \frac{2}{\exp\left(\sqrt{\frac{s}{D}}L\right) + \exp\left(-\sqrt{\frac{s}{D}}L\right)} J^{\mathrm{r}}(s) + \frac{\exp\left(\sqrt{\frac{s}{D}}L\right) - \exp\left(-\sqrt{\frac{s}{D}}L\right)}{\exp\left(\sqrt{\frac{s}{D}}L\right) + \exp\left(-\sqrt{\frac{s}{D}}L\right)} \sqrt{Ds} \frac{A}{RT} p^{\mathrm{b}}(s) \quad (14)$$

3.3.2. Approximating mass transport transfer function

Taylor's expansions of $\exp(\sqrt{(s/D)}L)$ and $\exp(-\sqrt{(s/D)}L)$ are

$$\exp\left(\sqrt{\frac{s}{D}}L\right) = 1 + \sqrt{\frac{s}{D}}L + \frac{1}{2}\frac{s}{D}L^2 + \frac{1}{6}\frac{s^{3/2}}{D^{3/2}}L^3 + \frac{1}{24}\frac{s^2}{D^2}L^4 + O\left(\sqrt{\frac{s}{D}}L\right),$$

$$\exp\left(-\sqrt{\frac{s}{D}}L\right) = 1 - \sqrt{\frac{s}{D}}L + \frac{1}{2}\frac{s}{D}L^2 - \frac{1}{6}\frac{s^{3/2}}{D^{3/2}}L^3 + \frac{1}{24}\frac{s^2}{D^2}L^4 + O\left(\sqrt{\frac{s}{D}}L\right)$$

Substituting them into Eqs. (13) and (14), and neglecting higher order term yield:

$$p^{\mathrm{tpb}}(s) = G_{\mathrm{Jp}} J^{\mathrm{r}}(s) + G_{\mathrm{pp}} p^{\mathrm{b}}(s),$$
$$J^{\mathrm{s}}(s) = G_{\mathrm{JJ}} J^{\mathrm{r}}(s) + G_{\mathrm{pJ}} p^{\mathrm{b}}(s) \quad (15)$$

where

$$G_{\mathrm{Jp}} = \frac{-\frac{L}{D} - \frac{L^3}{6D^2}s}{1 + \frac{L^2}{2D}s + \frac{L^4}{24D^2}s^2}\frac{RT}{A},$$

$$G_{\mathrm{pp}} = \frac{1}{1 + \frac{L^2}{2D}s + \frac{L^4}{24D^2}s^2}, \quad G_{\mathrm{JJ}} = \frac{1}{1 + \frac{L^2}{2D}s + \frac{L^4}{24D^2}s^2},$$

$$G_{\mathrm{pJ}} = \frac{Ls}{1 + \frac{L^2}{2D}s + \frac{L^4}{24D^2}s^2}\frac{A}{RT}$$

p^{tpb} is the partial pressure in the vicinity of tpbs, p^{b} the partial pressure in gas bulks, J^{s} the gas flow into the outer surface of porous material, J^{r} the gas consumption or water production rate at tpbs, L the layer thickness, A the cell area, D the effective diffusion coefficient, R the gas constant, and T is the temperature. So dynamic behavior of partial pressures in the vicinity of tpbs and gas flows at electrode surface can be determined uniquely by the behaviors of gas consumption rate and bulk pressure without relying on concentration distribution along the diffusion path.

In this dynamics description, only two parameters are involved. The first one is the thickness of the diffusion layer L. It depends on flow velocity, and can be calculated according to fluid mechanics. The second parameter is diffusion coefficient D. It can be calculated from correlation equations [24].

3.3.3. Diffusion coefficient

In porous materials, the effective diffusion coefficient is adjusted [24]:

$$D_{\mathrm{eff}} = \frac{\varepsilon}{\tau}D \quad (16)$$

where ε is the porosity, τ the tortuosity of porous materials, and $D$is the total diffusion coefficient.

Considering the Knudsen diffusion, the total diffusion coefficient is [24]:

$$\frac{1}{D} = \frac{1}{D_{12}} + \frac{1}{D_{\mathrm{k}}} \quad (17)$$

where D_{12} is the binary diffusion coefficient, and D_{k} is the Knudsen diffusion coefficient. If pores are large enough, Knudsen diffusion can be neglected [24].

The binary diffusion coefficient D_{12} is modeled by the Fuller's correlation [24]:

$$D_{12} = \frac{1.013^{-2}T^{1.75}\left(\frac{1}{M_1} + \frac{1}{M_2}\right)^{0.5}}{P[(\sum \nu_i)_1^{1/3} + (\sum \nu_i)_2^{1/3}]^2} \quad (18)$$

where T is the temperature, M_1 and M_2 are the mole mass of gases 1 and 2, $(\sum \nu_i)_1$ and $(\sum \nu_i)_2$ are the diffusional volumes of gases 1 and 2, respectively, and P is the total pressure. Good agreement between the Fuller's correlation and measurements has been reported in [25].

3.4. Voltage

As described before, fuel cell's voltage output is affected by gas partial pressures and is reduced by concentration loss, activation loss and ohmic loss. The dynamic behavior of the voltage is also affected by these factors.

In fact, because reactions take place at tpbs, it is partial pressures in the vicinity of tpbs that affect the EMF. The more appropriate expression of Nernst equation should be

$$E = E^0 + \frac{RT}{2F}\ln\left(\frac{p_{\mathrm{H_2}}^{\mathrm{tpb}}(p_{\mathrm{O_2}}^{\mathrm{tpb}})^{1/2}}{p_{\mathrm{H_2O}}^{\mathrm{tpb}}}\right) \quad (19)$$

where $p_{\mathrm{H_2}}^{\mathrm{tpb}}$, $p_{\mathrm{O_2}}^{\mathrm{tpb}}$, and $p_{\mathrm{H_2O}}^{\mathrm{tpb}}$ are the partial pressures in the vicinity of tpbs.

The H_2/O_2 consumptions lead to their concentration reductions in the vicinity of tpbs. The voltage drop caused by this kind of concentration reductions is named as concentration loss in the literature and is usually corrected by a static concentration loss term.

The activation loss is the potential consumed to overcome the activation energy barrier. It is normally described by the Butler–Volmer correlation [20]:

$$i = i_0 \left\{ \exp\left(\beta \frac{nF\eta_{\text{act}}}{RT}\right) - \exp\left[-(1-\beta)\frac{nF\eta_{\text{act}}}{RT}\right]\right\} \quad (20)$$

where β is the transfer coefficient and i_0 the exchange current. The transfer coefficient is usually taken as 0.5 for the fuel cell application [20].

When $\beta = 0.5$, the activation loss can be solved from Eq. (20):

$$\eta_{\text{act,a}} = \frac{2RT}{nF}\sinh^{-1}\left(\frac{i}{2i_{0,\text{a}}}\right),$$
$$\eta_{\text{act,c}} = \frac{2RT}{nF}\sinh^{-1}\left(\frac{i}{2i_{0,\text{c}}}\right) \quad (21)$$

The exchange currents depend on the activation energy, temperature, and partial pressures. They can be calculated as [17]:

$$i_{0,\text{a}} = 7\times 10^9\ \text{A}\left(p_{\text{H}_2}^{\text{tpb}} p_{\text{H}_2\text{O}}^{\text{tpb}}\right)\exp\left(-\frac{E_{\text{act,a}}}{RT}\right),$$
$$i_{0,\text{c}} = 7\times 10^9\ \text{A}\left(p_{\text{O}_2}^{\text{tpb}}\right)^{0.25}\exp\left(-\frac{E_{\text{act,c}}}{RT}\right) \quad (22)$$

where $E_{\text{act,a}}$, $E_{\text{act,c}}$ are anode and cathode activation energy, respectively.

Compensating the activation loss, the irreversible voltage is

$$E = E^0 + \frac{RT}{2F}\ln\left(\frac{p_{\text{H}_2}^{\text{tpb}}(p_{\text{O}_2}^{\text{tpb}})^{1/2}}{p_{\text{H}_2\text{O}}^{\text{tpb}}}\right) - \eta_{\text{act,a}} - \eta_{\text{act,c}} \quad (23)$$

with $E^0 = 1.273 - 2.7645\times 10^{-4}\,\text{T}$ [17].

3.5. Inherent impedance

When current flows through the inherent impedance, voltage is reduced. The voltage drop is called Ohmic loss. The dynamic characteristics of the inherent impedance also affect the dynamic voltage behavior of the fuel cell.

Inherent impedance of SOFC is complex. Basically, it consists of two charge capacitance processes and three resistance processes: anode charge double layer capacitance, cathode charge double layer capacitance, ohmic resistance, grain boundary resistances and electrode reaction resistances. Because their dynamic behaviors are similar to RC circuits, the inherent impedance is usually modeled as equivalent RC circuits. A typical equivalent circuit to inherent impedance is shown in Fig. 4. Here R_e is the resistance of electrolyte, R_a and R_c represent the ohmic resistances of anode and cathode, R_{cta} and R_{ctc} represent the charge transfer resistances, respectively, and C_{dla} and C_{dlc} represent the charge double layer capacitors between anode, cathode and electrolyte.

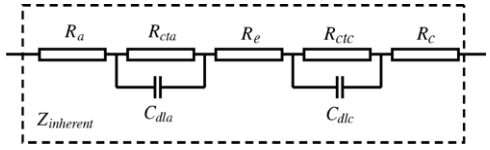

Fig. 4. Equivalent circuit of inherent impedance.

3.6. Equivalent circuit

Theoretically, impedance spectra plane plot indicates two semicircles for the impedance shown in Fig. 4 [10]. In SOFC, neglecting diffusion impedance, these two semicircles are merged to one distorted semicircle [12]. This means that the whole inherent impedance can be approximated by one RC unit. In another aspect, potential difference is produced between tpbs, inside the two metal electrode layers, as shown in Fig. 1. That means voltage fluctuation due to potential change is smoothed by the double layer capacitance. So a reasonable equivalent circuit of a SOFC cell is shown in Fig. 5, where R_o is the total ohmic resistance in the inherent impedance, R_{ct} is the total charge transfer resistance, and C_{ct} is the approximated charge transfer capacitance. These three parameters can be identified from impedance spectral plan plot [10] or Bode plot [12].

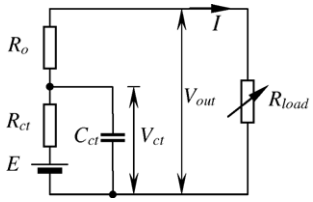

Fig. 5. Equivalent circuit of a single fuel cell.

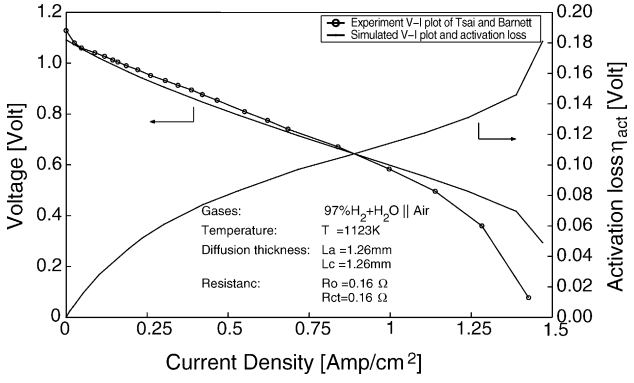

Fig. 6. Comparison of simulated and experiment *V–I* plot.

This equivalent circuit is different from the one shown in [8], where the ideal battery is connected in serial with a RC pair. That equivalent circuit shows derivative effect on battery potential change. The derivative phenomenon on fuel cell has not been observed and reported in literature. The model shown in Fig. 5 is an integral circuit. It smooths the voltage output, and appears to be more reasonable.

The dynamic behavior of the voltage output based on the equivalent circuit is therefore determined by

$$\dot{V}_{\rm ct} = \frac{1}{R_{\rm ct}C_{\rm ct}}E - \frac{1}{R_{\rm ct}C_{\rm ct}}V_{\rm ct} - \frac{1}{C_{\rm ct}}I,$$
$$V_{\rm out} = V_{\rm ct} - iR_{\rm o}, \qquad i = \frac{V_{\rm ct}}{R_{\rm o}+R_{\rm load}} \tag{24}$$

3.7. Model in the state-space form

Converting the transfer function form of dynamic relations shown in Eq. (15) to differential equation form, the dynamic behaviors can be shown as:

- Hydrogen consumption rate:

$$\dddot{J}^{\rm s}_{\rm H_2} = -h_1 J^{\rm s}_{\rm H_2} - h_2 \dot{J}^{\rm s}_{\rm H_2} + h_1 J^{\rm r}_{\rm H_2} + h_3 \frac{A}{RT}\dot{p}^{\rm b}_{\rm H_2} \tag{25}$$

and partial pressure in the vicinity of anode tpb:

$$\ddot{p}^{\rm tpb}_{\rm H_2} = -h_1 p^{\rm tpb}_{\rm H_2} - h_2 \dot{p}^{\rm tpb}_{\rm H_2} - h_4 \frac{RT}{A} J^{\rm r}_{\rm H_2} - \frac{4}{L_{\rm a}}\frac{RT}{A}\dot{J}^{\rm r}_{\rm H_2} + h_1 p^{\rm b}_{\rm H_2} \tag{26}$$

where $h_1 = 24D^2_{\rm H_2}/L^4_{\rm a}$, $h_2 = 12D_{\rm H_2}/L^2_{\rm a}$, $h_3 = 24D^2_{\rm H_2}/L^3_{\rm a}$, $h_4 = 24D_{\rm H_2}/L^3_{\rm a}$.

- Oxygen consumption rate:

$$\dddot{J}^{\rm s}_{\rm O_2} = -o_1 J^{\rm s}_{\rm O_2} - o_2 \dot{J}^{\rm s}_{\rm O_2} + o_1 J^{\rm r}_{\rm O_2} + o_3 \frac{A}{RT}\dot{p}^{\rm b}_{\rm O_2} \tag{27}$$

and partial pressure in the vicinity of cathode tpb:

$$\ddot{p}^{\rm tpb}_{\rm O_2} = -o_1 p^{\rm tpb}_{\rm O_2} - o_2 \dot{p}^{\rm tpb}_{\rm O_2} - o_4 \frac{RT}{A} J^{\rm r}_{\rm O_2} - \frac{4}{L_{\rm c}}\frac{RT}{A}\dot{J}^{r}_{\rm O_2} + o_1 p^{\rm b}_{\rm O_2} \tag{28}$$

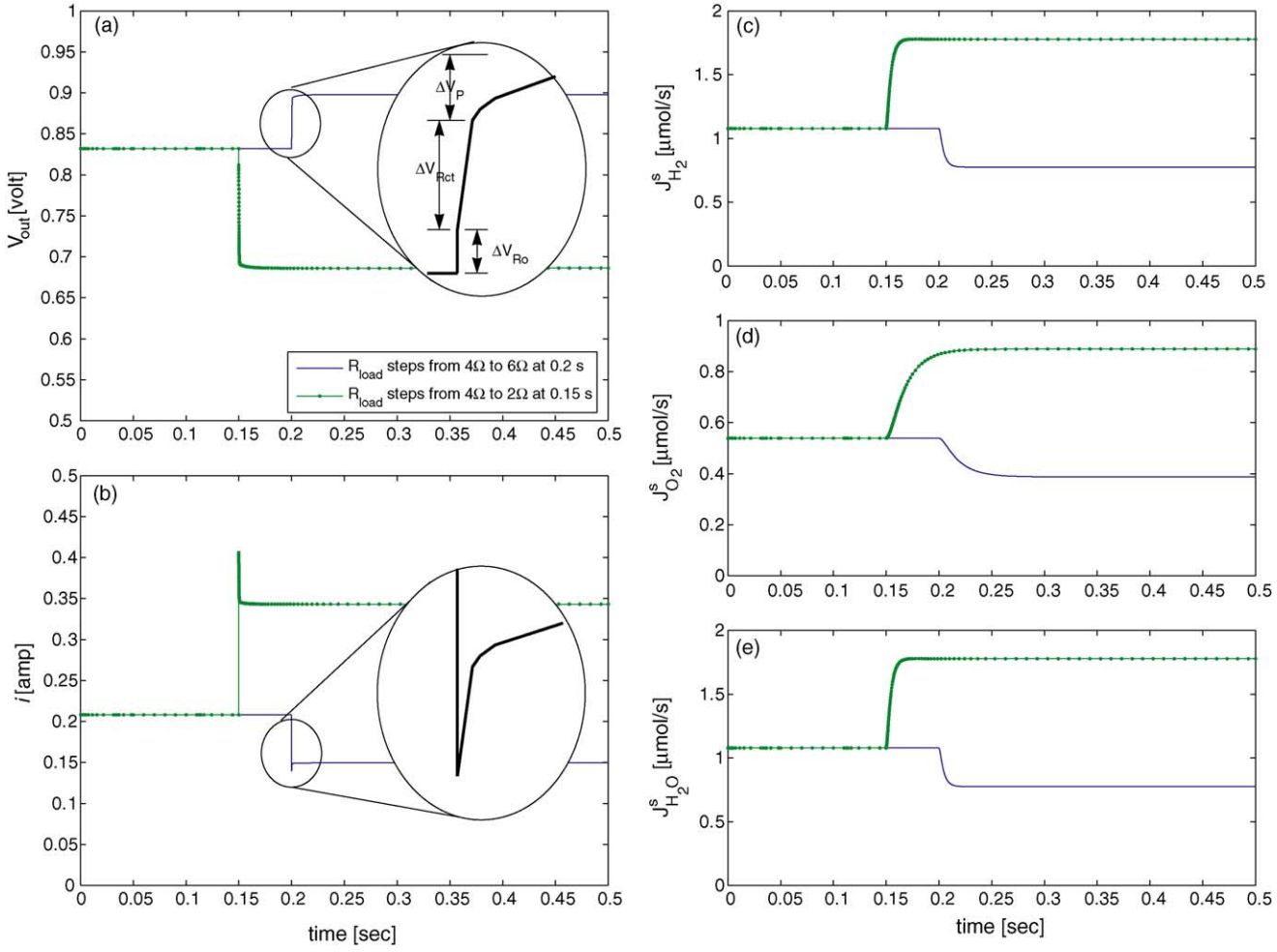

Fig. 7. Step responses of SOFC, when load resistance changes.

where $o_1 = 24D^2_{O_2}/L^4_c$, $o_2 = 12D_{O_2}/L^2_c$, $o_3 = 24D^2_{O_2}/L^3_c$, $o_4 = 24D_{O_2}/L^3_c$.

- Water vapor production rate:

$$\ddot{J}^s_{H_2O} = -w_1 J^s_{H_2O} - w_2 \dot{J}^s_{H_2O} + w_1 J^r_{H_2O} + w_3 \frac{A}{RT} \dot{p}^b_{H_2O} \tag{29}$$

and partial pressure in the vicinity of anode tpb:

$$\ddot{p}^{tpb}_{H_2O} = -w_1 p^{tpb}_{H_2O} - w_2 \dot{p}^{tpb}_{H_2O} - w_4 \frac{RT}{A} J^r_{H_2O} - \frac{4}{L_a} \frac{RT}{A} \dot{J}^r_{H_2O} + w_1 p^b_{H_2O} \tag{30}$$

where $w_1 = 24D^2_{H_2O}/L^4_a$, $w_2 = 12D_{H_2O}/L^2_a$, $w_3 = 24D^2_{H_2O}/L^3_a$, $w_4 = 24D_{H_2O}/L^3_a$.

First order derivative of an input variable can be approximated by [26]:

$$sU(s) \approx K\left(1 - \frac{1}{\frac{1}{K}s + 1}\right) U(s) \tag{31}$$

in the differential equation form:

$$\dot{u} = Ku - v, \qquad \dot{v} = K^2 u - Kv \tag{32}$$

where v is a intermediate variable. K is the approximation factor, usually greater than 10.

Define the input vector as

$$\mathbf{u} = [\, R_{load} \;\; p^b_{H_2} \;\; p^b_{O_2} \;\; p^b_{H_2O} \,]^T \tag{33}$$

output vector as

$$\mathbf{y} = [\, V_{out} \;\; i \;\; J^s_{H_2} \;\; J^s_{O_2} \;\; J^s_{H_2O} \,]^T \tag{34}$$

Introduce intermediate variables v_{H_2}, v_{O_2}, v_{H_2O}, v_R and define states as

$$\mathbf{x} = [\, V_{ct} \;\; J^s_{H_2} \;\; \dot{J}^s_{H_2} \;\; v_{H_2} \;\; J^s_{O_2} \;\; \dot{J}^s_{O_2} \;\; v_{O_2} \;\; J^s_{H_2O} \;\; \dot{J}^s_{H_2O} \;\; v_{H_2O} \;\; p^{tpb}_{H_2} \;\; \dot{p}^{tpb}_{H_2} \;\; p^{tpb}_{O_2} \;\; \dot{p}^{tpb}_{O_2} \;\; p^{tpb}_{H_2O} \;\; \dot{p}^{tpb}_{H_2O} \;\; v_R \,]^T \tag{35}$$

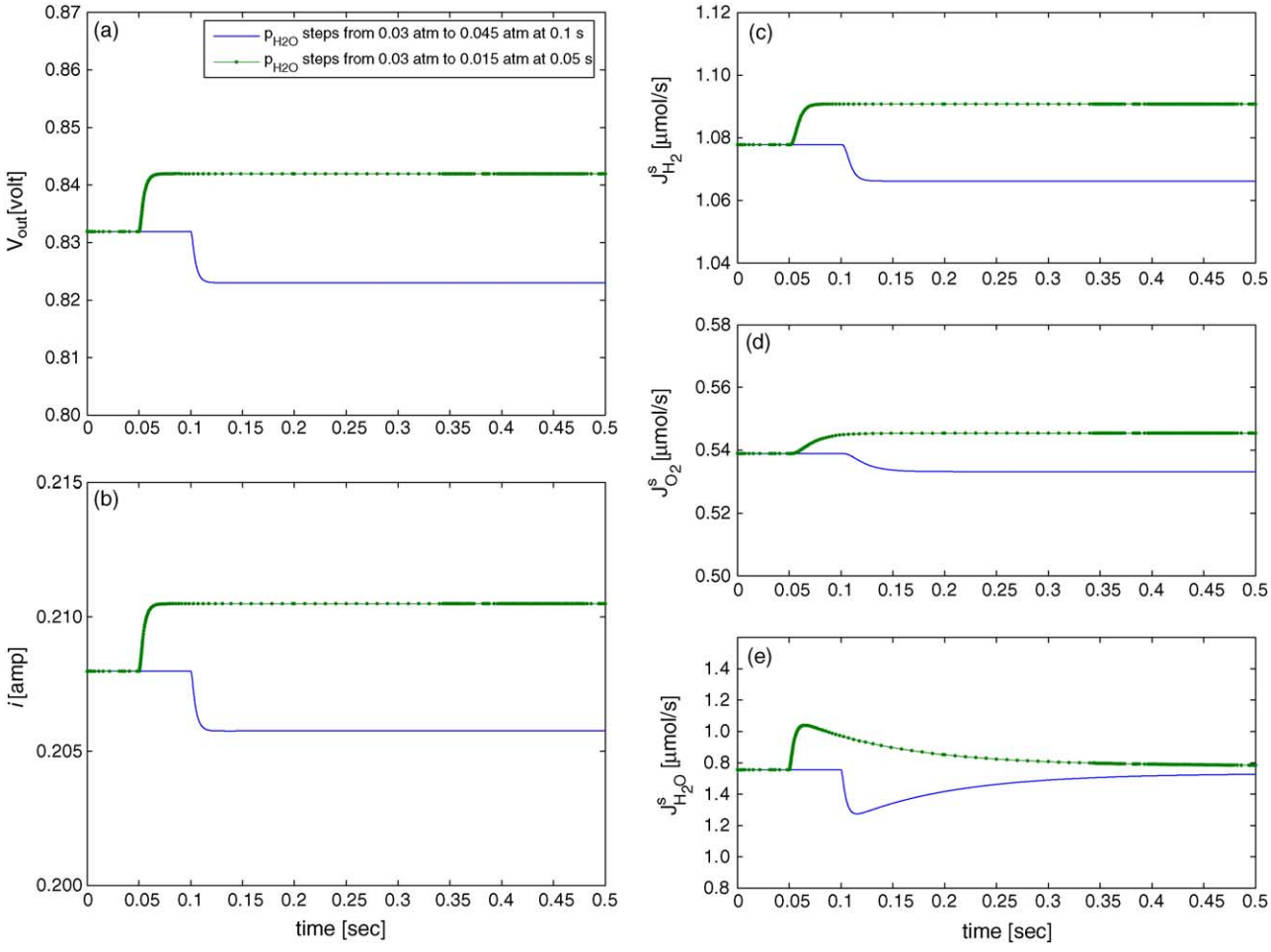

Fig. 8. Step responses of SOFC, when hydrogen pressure changes.

Combine Eqs. (23)–(32), the state-space model is given by

State equations:

$$\dot{x}_1 = \frac{1}{R_{ct}C_{ct}}E - \frac{1}{R_{ct}C_{ct}}x_1 - \frac{1}{C_{ct}}\frac{x_1}{u_1 + R_o}$$

$$\dot{x}_2 = x_3$$

$$\dot{x}_3 = -h_1x_2 - h_2x_3 + h_1\frac{1}{2F}\frac{x_1}{u_1 + R_o} + h_3\frac{A}{RT}(Ku_2 - x_4)$$

$$\dot{x}_4 = K^2u_2 - Kx_4$$

$$\dot{x}_5 = x_6$$

$$\dot{x}_6 = -o_1x_5 - o_2x_6 + o_1\frac{1}{4F}\frac{x_1}{u_1 + R_o} + o_3\frac{A}{RT}(Ku_3 - x_7)$$

$$\dot{x}_7 = K^2u_3 - Kx_7$$

$$\dot{x}_8 = x_9$$

$$\dot{x}_9 = -w_1x_8 - w_2x_9 + w_1\frac{1}{2F}\left(\frac{-x_1}{u_1 + R_o}\right) + w_3\frac{A}{RT}(Ku_4 - x_{10})$$

$$\dot{x}_{10} = K^2u_4 - Kx_{10}$$

$$\dot{x}_{11} = x_{12}$$

$$\dot{x}_{12} = -h_1x_{11} - h_2x_{12} - h_4\frac{RT}{A}\frac{1}{2F}\frac{x_1}{u_1 + R_o} - \frac{RT}{A}\frac{4}{L_a}\frac{1}{2F}\left[\frac{\dot{x}_1}{u_1 + R_o} - \frac{x_1}{(u_1 + R_o)^2}(Ku_1 - x_{17})\right] + h_1u_2$$

$$\dot{x}_{13} = x_{14}$$

$$\dot{x}_{14} = -o_1x_{13} - o_2x_{14} - o_4\frac{RT}{A}\frac{1}{4F}\frac{x_1}{u_1 + R_o} - \frac{RT}{A}\frac{4}{L_c}\frac{1}{4F}\left[\frac{\dot{x}_1}{u_1 + R_o} - \frac{x_1}{(u_1 + R_o)^2}(Ku_1 - x_{17})\right] + o_1u_3$$

$$\dot{x}_{15} = x_{16}$$

$$\dot{x}_{16} = -w_1x_{15} - w_2x_{16} - w_4\frac{RT}{A}\frac{1}{2F}\left(\frac{-x_1}{u_1 + R_o}\right) - \frac{RT}{A}\frac{4}{L_a}\frac{1}{2F}\left[-\frac{\dot{x}_1}{u_1} + \frac{x_1}{(u_1 + R_o)^2}(Ku_1 - x_{17})\right] + w_1u_4$$

$$\dot{x}_{17} = K^2u_1 - Kx_{17}$$

Output equations:

$$y_1 = x_1 - \frac{R_o}{u_1 + R_o}x_1$$

$$y_2 = \frac{x_1}{u_1 + R_o}$$

$$y_3 = x_2$$

$$y_4 = x_5$$

$$y_5 = x_8$$

or in a compact form:

$$\dot{\mathbf{x}} = f(\mathbf{x}, \mathbf{u}), \qquad \mathbf{y} = g(\mathbf{x}, \mathbf{u}) \tag{36}$$

4. Parameters

This state-space model involves several parameters. Numerical values and their sources are listed in Table 2. These are default parameters for our model. However, since these parameters are collected from a variety of references, in the validation of the model with a specific data set, some of the default parameters have to be adjusted to the published specific parameters for a meaningful comparison.

5. Simulation results

Simulation is done according to the developed state-space model. Steady state and transient behaviors of SOFC at different inputs and disturbances are investigated through the simulation.

5.1. Steady state output and model validation

Dynamic data that are useful for the validation of the developed model are very limited in the literature. We will validate

Table 2
Parameters used in simulation

Symbol	Description	Source
$L_a = 1\,\text{mm}$	Thickness of anode diffusion layer	*V–I* plot [27]
$L_c = 1\,\text{mm}$	Thickness of cathode diffusion layer	*V–I* plot [27]
$A = 1\,\text{cm}^2$	Fuel cell effective area	[27]
$R_{ct} = 0.9\,\Omega$	Charge transfer resistance	EIS test [12]
$R_o = 0.1\,\Omega$	Ohmic resistance	EIS test [12]
$C = 300\ \mu\text{F}$	Charge transfer capacitance	EIS test [12]
$E_{act,a} = 110\,\text{kJ mol}^{-1}$	Anode activation energy	[17]
$E_{act,a} = 120\,\text{kJ mol}^{-1}$	Cathode activation energy	[17]
$\varepsilon = 0.4$	Porosity	[24]
$\tau = 4$	Tortuosity	[24]
$(\sum \nu_i)_{H_2} = 7.07$	Diffusional volume	[24]
$(\sum \nu_i)_{H_2O} = 12.7$	Diffusional volume	[24]
$(\sum \nu_i)_{O_2} = 16.6$	Diffusional volume	[24]
$(\sum \nu_i)_{N_2} = 17.9$	Diffusional volume	[24]
$T = 1223\,\text{K}$	Work temperature	[12]
$p^b_{H_2} = 0.97\,\text{atm}$	Input partial pressure	[12]
$p^b_{air} = 1\,\text{atm}$	Cathode pressure	[12]
$p^b_{H_2O} = 0.03\,\text{atm}$	Input partial pressure	[12]

the model according to the experiment results of Wagner et al. [12] and Tsai and Barnett [27] respectively.

Wagner et al. [12] investigated the effect of diffusion of SOFC, and the dynamic properties are shown by EIS Bode plot. Given 3% humidified H_2, pure O_2 and infinite large load resistance R_{load}, at 1223 K, the simulated steady state OCV is 1117 mV. This is in a good agreement with measured OCV of 1114 mV by Wagner et al. [12] under the same condition. Because Wagner et al. [12] did not present the thickness of diffusion layers, the experiment *V–I* plot can not be used to verify the dynamic model.

The comparison of the simulated steady state *V–I* outputs and the experiment result of Tsai and Barnett [27] is shown in Fig. 6.

Tsai and Barnett [27] did not give the thickness of the diffusion layer directly. When i reaches the limit i_l, at which the gas supply rate is maximum, thickness of the diffusion layer can be calculated by the relation [27]:

$$i_l = 4FJ^r_{O_2} = 4FAD_{O_2}\frac{C^b - 0}{L_c} \tag{37}$$

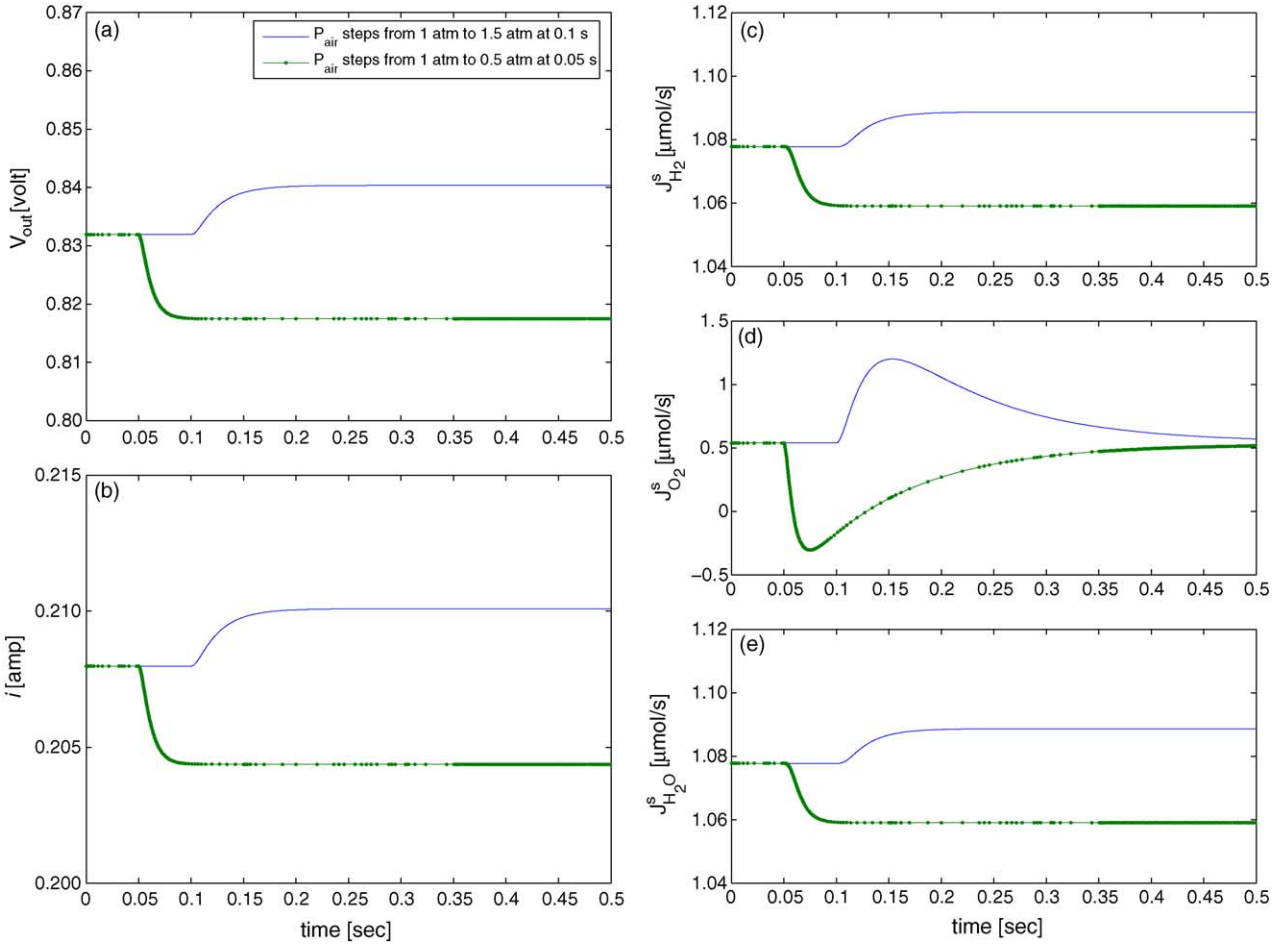

Fig. 9. Step responses of SOFC, when air pressure changes.

Using Eq. (37), the thickness is calculated as $L_c = 1.26 \times 10^{-3}$ m. Because anode diffusion does not contribute to the limitation, the thickness in anode can not be calculated. L_a is assumed same as L_c in the simulation. The inherent resistance read from the EIS test of Tsai and Barnett [27] is $R_o = 0.16\,\Omega$ and $R_{ct} = 0.16\,\Omega$ at 1123 K.

The *V–I* plot shows that the simulated result is overall in agreement with the experiment data with some error. A main reason for the error is the unavoidable model parameter error used in the simulation. They are collected from different sources and are dispersed in a wide range in different literatures.

5.2. Step responses due to R_{load} step changes

As shown in Fig. 7a, when load resistance has step changes, current will change immediately according to Ohm's law. Voltage on the pure ohmic inherent resistance R_o also changes at once. The result is an immediate rise of V_{out}. Then, for the reason of charge transfer capacity, voltage on the charge transfer resistance R_{ct} changes slowly. V_{out} then rises slowly to the final value [8]. The response can therefore be divided into three stages, immediate change, then fast response and slow response following the fast response.

For the specific SOFC investigated by Wagner et al. [12], the charge transfer capacity is around several hundred microfarads. The charge transfer resistance is around 1 Ω. So the time constant is less than 1 ms. The effect of charge transfer capacity can not be distinguished from the immediate rise of voltage. The fast response in Fig. 7a is actually the summation of the changes of voltage drop on R_o and R_{ct}.

The slow response following the fast response is caused by the slow changes of concentration at the vicinity of tpbs. When J^r changes simultaneously with current change, p^{tpb} changes at a slow rate. The behaviors are determined by Eqs. (26), (28) and (30). Thus, according to Nernst relation, E responses slowly to the new value. Assume the diffusion thickness $L_a = L_c = 1$ mm, simulated time constant of the slower voltage response is around 0.02 s. It is in good agreement with Wagner's experiment results [12]. In [12], a concentration impedance from 10 Hz is observed

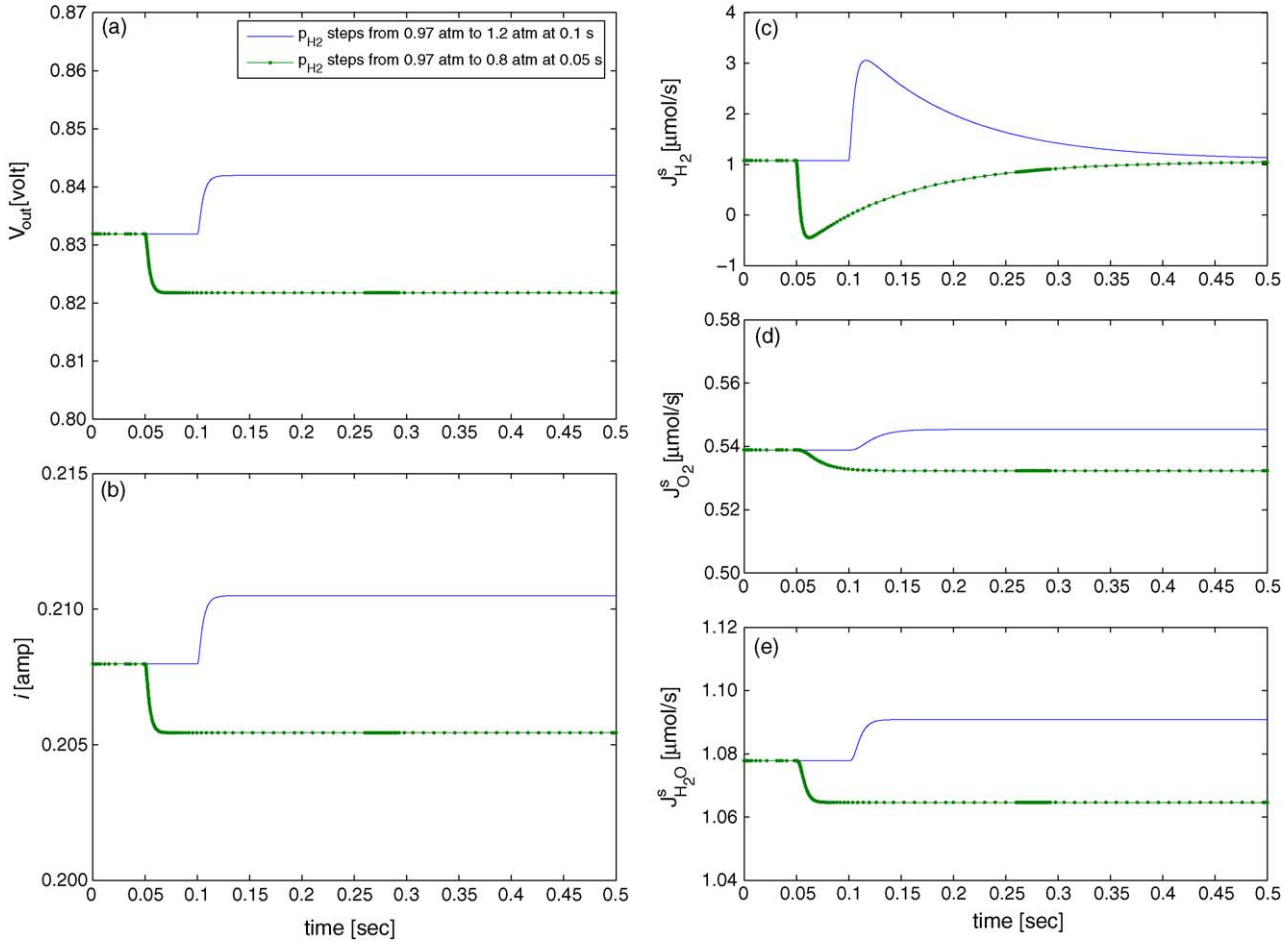

Fig. 10. Step responses of SOFC, when water vapor pressure in anode gas changes.

in the EIS test Bode plot. The time constant is identified as 0.018 s.

The voltage output step response is similar to the current interrupt test result shown in [8], where the dynamic behavior of V_{out} is explained only by the charge transfer resistance and capacitance. Contributions from concentration changes in the vicinity of tpbs are not noticed. The simulation results show that it is concentration changes in the vicinity of tpbs that are the main reason for the slow voltage rise behavior. The current response is shown in Fig. 7b which is related to the voltage response by Ohm's law.

Reactant consumption rates at diffusion layer surface respond at a slow rate, as shown in Fig. 7c–e. Time constant of oxygen is different from that of hydrogen and water. This different response processes lead to different behaviors of reactant partial pressures in a fuel cell stack and in turn affect the electrical power output. The different transient responses will also lead to the change of pressure difference between anode side and cathode side. The reason for these slow dynamic responses is the existence of the diffusion layers. The diffusion layer plays a role like a buffer, which damps the response of fuel transportation to tpbs.

5.3. Reactant partial pressure disturbances

Partial pressure disturbances in gas bulk lead to electrical power output fluctuation and change the reaction rate. Step responses due to hydrogen, air, and water vapor pressures are shown in Figs. 8–10, respectively. Simulation results show that influences from pressure disturbances in gas bulks on voltage and current are relatively small. That is because the electrical power output is controlled mainly by reaction and load resistance, and the existence of the buffer effect of the diffusion layer.

5.4. Effect of concentration loss

When load resistance moves to a small value, it leads SOFC to the concentration loss dominant region,

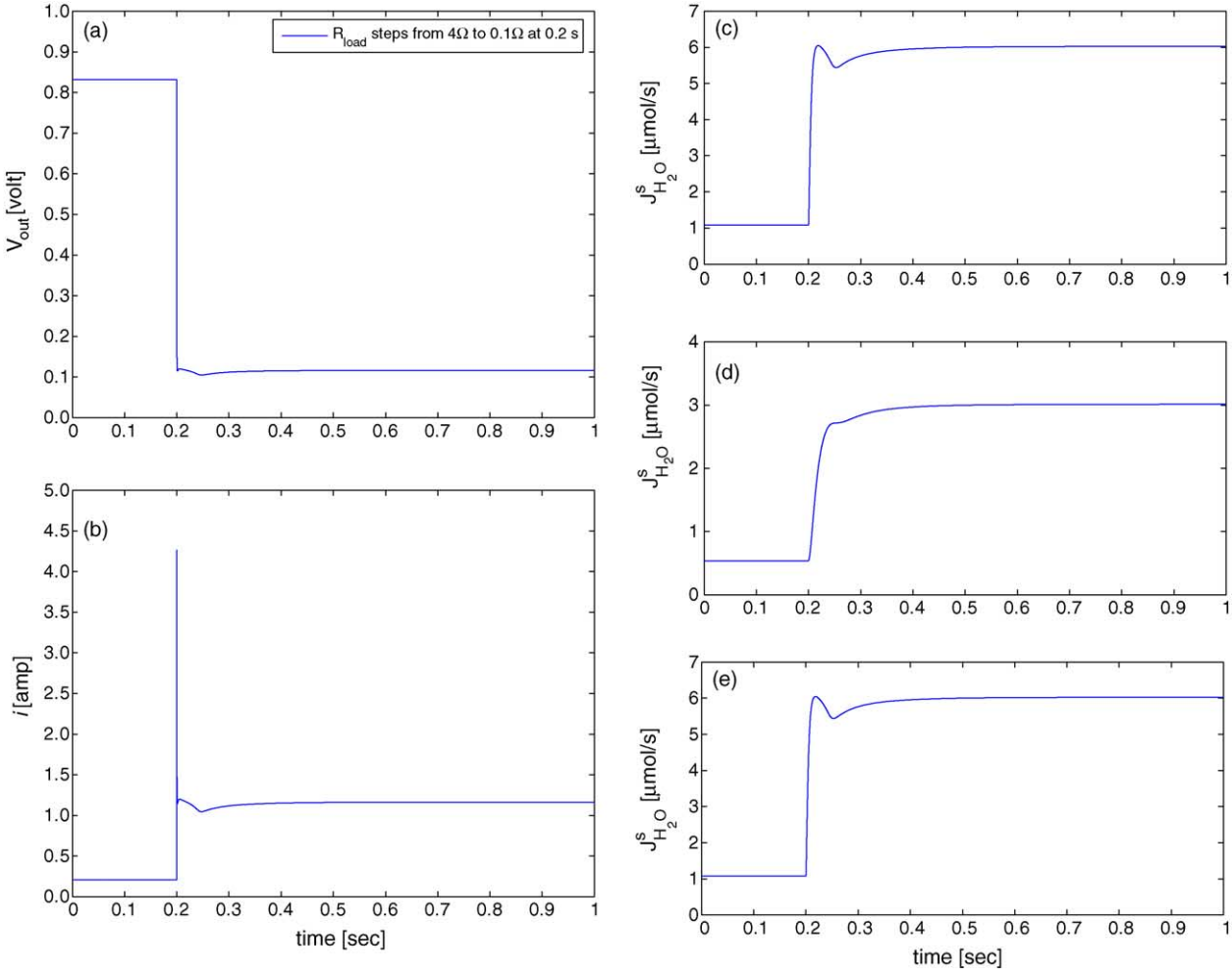

Fig. 11. Step responses of SOFC, when it enters concentration loss range.

the dynamic behaviors of SOFC is considerably different from that in ohmic loss range, as shown in Fig. 11. The transient response processes behave a high order dynamics.

Simulation result shows that in the air fueled SOFC, it is the oxygen supply that is the main resource of the concentration loss. Because oxygen fraction in air is only around 21%. Oxygen supply also plays the main role in the dynamic behavior of SOFC, since its diffusion coefficient is smaller than that of hydrogen and water.

5.5. Effect of diffusion layers

Simulation result shows that the thickness of the diffusion layer has strong effect on properties of SOFC. With the increasing of the thickness, time constants of the dynamics increase. The resistance from diffusion also increases. The effect is shown in Fig. 12.

Diffusion layers in fuel cell consist of not only electrode layer, but also boundary layer. The thicknesses are affected by the status of flow bulks, especially the flow velocity. So the thicknesses of diffusion layers may vary within a large range.

5.6. Effect of temperature

Given different temperatures, the simulation shows that compared to its effect on SOFCs dynamics, temperature has larger effect on the voltage output, as shown in Fig. 13.

Temperature affects the Gibb's free energy $\Delta\bar{g}_f$, and thus Nernst voltage. It also affects the conductivity of electrolyte, electrodes and connectors. Simulation shows that the effect of temperature on Gibb's free energy and the Nernst voltage is much larger than on other factors.

As shown in Fig. 13, the effect of temperature on the transient property of the diffusion response is negligible.

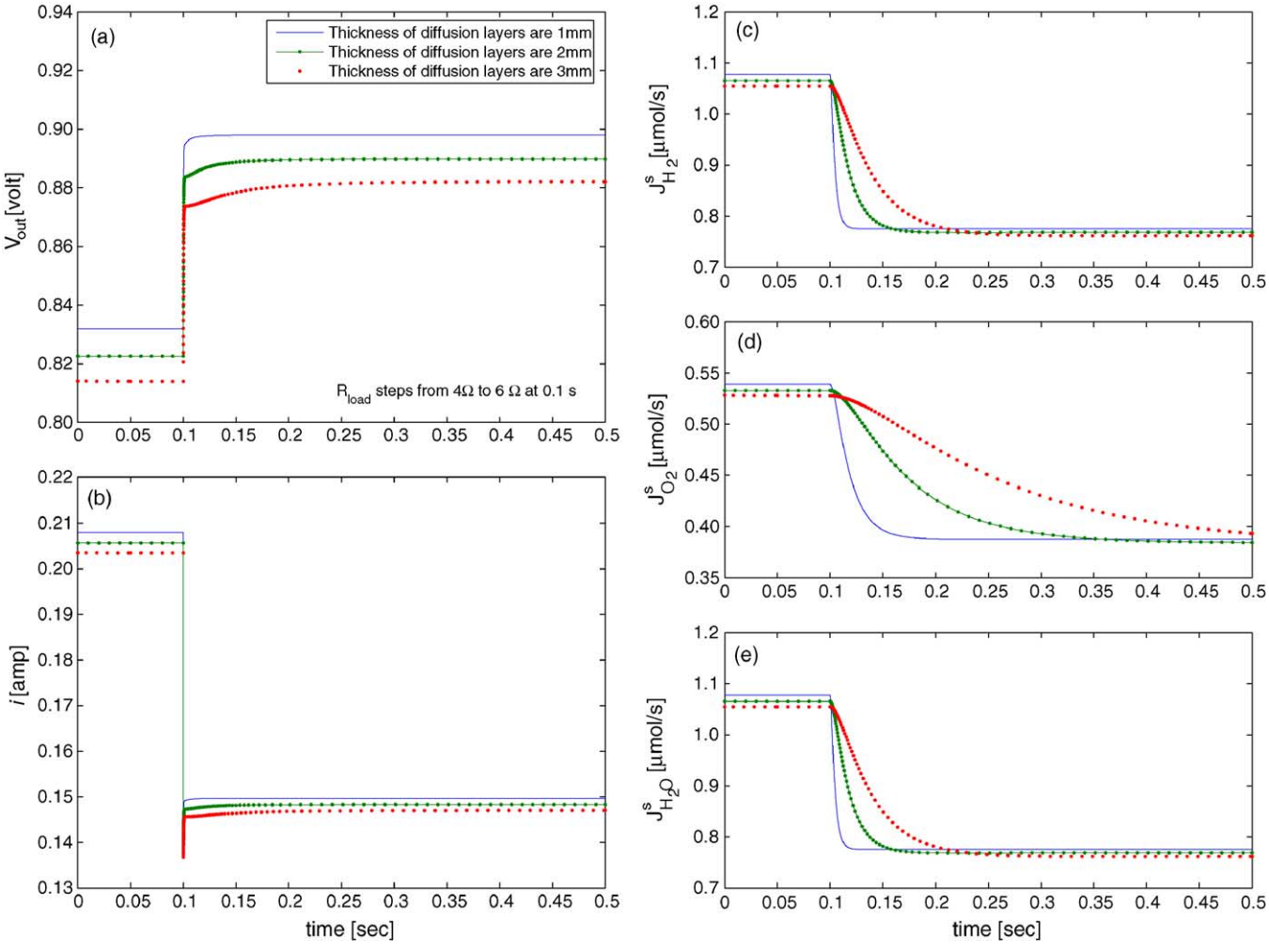

Fig. 12. Effect of diffusion layer thickness on step responses of SOFC.

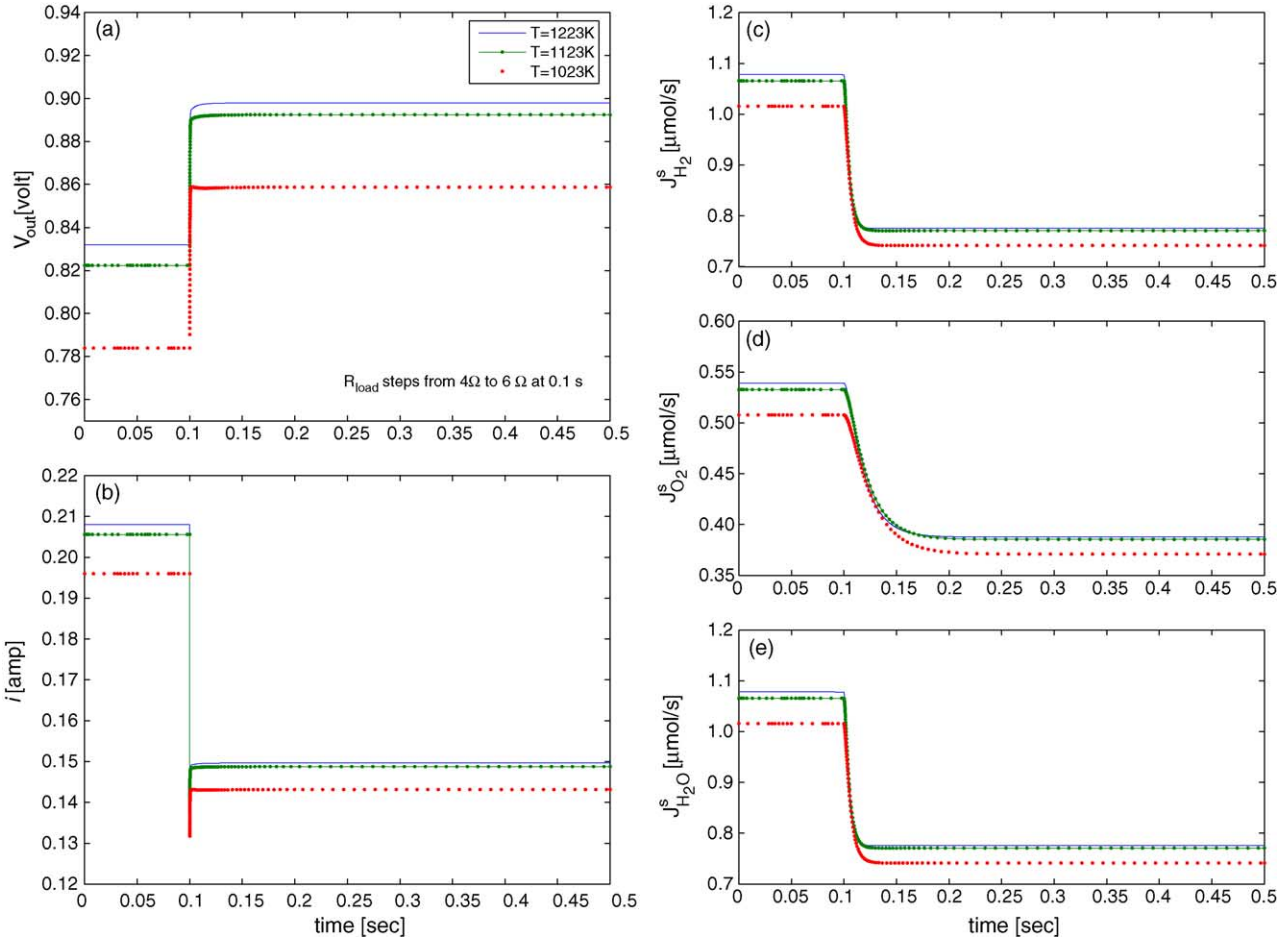

Fig. 13. Effect of temperature on step responses of SOFC.

6. Conclusion

A dynamic model of solid oxide fuel cell (SOFC) with a focus on the diffusion process at cell-level is derived in the paper. The species dynamics is built in the form of the state-space model. Dynamic properties of SOFC are shown through simulations. It demonstrates that diffusion processes in porous layers play an important role in the dynamic behavior of SOFC. They affect concentrations in the vicinity of triple phase boundary (tpb), and thus the electrical properties.

Simulation shows that it is the dynamic behavior of partial pressures in the vicinity of tpbs contribute more to the slow rise of voltage in the step response test and current interrupt experiment, not the charge transfer capacitance. Given different diffusion thicknesses, it is found that the voltage output and dynamic behavior of gas consumption rates are affected greatly by the thicknesses of the diffusion layers. Simulations also indicates that temperature has large effect on the voltage output.

Acknowledgement

This work is supported in part by NSERC.

References

[1] Y. Yamamura, S. Kawasaki, H. Sakai, Molecular dynamics analysis of ionic conduction mechanism in yttria-stabilized zirconia, Solid State Ionics 126 (1999) 181–189.
[2] T.P. Perumal, V. Sridhar, K.P.N. Murthy, Molecular dynamics simulations of oxygen ion diffusion in yttria-stabilized zirconia, Physica A 309 (2002) 35–44.
[3] E. Achenbach, Three-dimensional and time dependent simulation of a planar solid oxide fuel cell stack, J. Power Sources 49 (1994) 333–348.
[4] E. Achenbach, Response of a solid oxide fuel cell to load change, J. Power Sources 57 (1995) 105–109.
[5] J. Padullés, G.W. Ault, J.R. McDonald, An integrated SOFC plant dynamic model for power systems simulation, J. Power Sources 86 (2000) 495–500.
[6] Y. Zhu, K. Tomsovic, Development of models for analyzing the load-following performance of microturbines and fuel cells, Electr. Power Syst. Res. 62 (2001) 1–11.
[7] K. Sedghisigarchi, A. Feliachi, Dynamic and transient analysis of power distribution systems with fuel cells—part I, IEEE Trans. Energy Conver. 19 (2) (2004) 423–428.
[8] J. Larminie, A. Dicks, Fuel Cell Systems Explained, 3rd ed., John Wiley & Sons Inc., Chichester, West Sussex, 2003.
[9] A. Mitterdorfer, L.J. Gauckler, Reaction kinetics of the Pt, O_2(g)|c-ZrO_2 system: precursor mediated adsorption, Solid State Ionics 117 (1999) 203–217.
[10] J.R. Macdonald, Impedance spectroscopy: Emphasizing solid materials and systems, John Wiley & Sons Inc., New York, 1987.

[11] M. Mogensen, S. Skaarup, Kinetic and geometric aspects of solid oxide fuel cell electrodes, Solid State Ionics 86–88 (1996) 1151–1160.
[12] N. Wagner, W. Schnurnberger, B. Müller, M. Lang, Electrochemical impedance spectra of solid-oxide fuel cells and polymer membrane fuel cells, Electrochim. Acta 43 (1998) 3785–3793.
[13] M.J. Jørgensen, S. Primdahl, M. Mogensen, Characterizationion of composite SOFC cathodes using electrochemical impedance spectroscopy, Electrochim. Acta 44 (1999) 4195–4201.
[14] A. Barbucci, R. Bozzo, G. Cerisola, P. Costamagna, Characterization of composite SOFC cathodes using electrochemical impedance spectroscopy. Analysis of Pt/YSZ and LSM/YSZ electrodes, Electrochim. Acta 47 (2002) 2183–2188.
[15] P. Holtappels, J. Bradley, J.T.S. Irvine, A. Kaiser, M. Mogensen, Electrochemical characterization of ceramic SOFC anodes, J. Electrochem. Soc. 148 (8) (2001) A923–A929.
[16] M.J. Jørgensen, M. Mogensen, Impedance of solid oxide fuel cell LSM/YSZ composite cathodes, J. Electrochem. Soc. 148 (5) (2001) A433–A442.
[17] S. Campanari, P. Iora, Definition sensitivity analysis of a finite volume SOFC model for a tubular cell geometry, J. Power Sources 132 (2004) 113–126.
[18] A. Mitterdorfer, L.J. Gauckler, Identification of the reaction mechanism of the Pt, O_2(g)|yttria-stabilized zirconia system. Part I. General framework, modelling, and structural investigation, Solid State Ionics 117 (1999) 187–202.
[19] A. Bieberle, L.J. Gauckler, Reaction mechanism of Ni pattern anodes for solid oxide fuel cells, Solid State Ionics 135 (2000) 337–345.
[20] S.H. Chan, K.A. Khor, Z.T. Xia, A complete polarization model of a solid oxide fuel cell and its sensitivity to the change of cell component thickness, J. Power Sources 93 (2001) 130–140.
[21] S.H. Chan, Z.T. Xia, Anode micro-model of solid oxide fuel cell, J. Electrochem. Soc. 148 (4) (2001) A388–A394.
[22] S.H. Chan, X.J. Chen, K.A. Khor, Cathode micromodel of solid oxide fuel cell, J. Electrochem. Soc. 151 (1) (2004) A164–A172.
[23] H. Wayland, Differential Equations Applied in Science and Engineering, D. Van Nostrand Company Ltd., Princeton, NJ, 1957.
[24] J.R. Welty, C.E. Wicks, R.E. Wilson, Fundamentals of momentum, heat and mass transfer, John Wiley & Sons Inc., New York, 1984.
[25] A. Solheim, In SOFC Micromodelling, An International Energy Agency SOFC Task Report, Swiss Federal Office of Energy, Brene, Switzerland, 1992, p. 9.
[26] D.E. Seborg, T.F. Edgar, D.A. Mellichamp, Process Dynamics and Control, 1st ed., John Wiley & Sons Inc., Singapore, 1989.
[27] T. Tsai, S.A. Barnett, Effect of LSM–YSZ cathode on thin-electrolyte solid oxide fuel cell performance, Solid State Ionics 93 (1997) 207–217.